# EFFECTS OF BACKING BOARD MATERIALS ON WOOD COMBUSTION PERFORMANCE

**Mathew J. Hagge - Kenneth M. Bryden - Mark A. Dietenberger**

## Abstract

Cone calorimeter tests show that backing board materials do not affect the ignition time, initial heat release rate, or the total heat released of combustion for redwood slabs. However, it has been observed that backing board materials alter combustion performance by altering the secondary heat release peak observed when the pyrolysis reaction front nears the unheated side of the wooden slab. This occurs because the presence of backing board materials provides different boundary conditions on the unheated side of the wooden slab. In this paper, a detailed pyrolysis model is used to examine the processes by which backing board materials alter the combustion performance. This model is validated using cone calorimeter data for redwood slabs, and is used to give a qualitative discussion of the impact of various backing board materials on combustion performance.

## INTRODUCTION

Studies using the standard burn test (ISO9705), the flame-spread test (Steiner tunnel test, ASTM E84), and cone calorimeter tests (ASTM E1354) have highlighted the need to account for backing materials when determining combustion performance. In a study using the cone calorimeter tests (Dietenberger, 1999), tests for southern yellow pine and redwood demonstrated that backing board materials can alter the heat release rate profile of a wooden slab. While the initial response and peak heat release rate depend on the external flux from the cone calorimeter, subsequent gas fluxes and heat release rates can be altered by backing board materials.

In cone calorimeter tests, a wooden slab is exposed to a constant external heat flux, combustion reactions occur with ambient air, and combustion performance in analyzed by measurements of heat release rate, mass loss, and gaseous products. For this paper, redwood slabs were exposed to a 35kW/$m^2$ or a 50kW/$m^2$ heat flux by a cone calorimeter. The redwood slabs were 19mm thick and had 7% moisture content on a dry basis. The measured heat release rates of combustion using cone calorimeter heat fluxes of 35 kW/$m^2$ and 50kW/$m^2$ are shown in Figures 1 and 2. The heat release rate typically consists of a large initial peak as the surface of the particle is rapidly pyrolyzed. The pyrolysis gases are driven out of the particle by pressurization within the particle, and once ignition occurs, gas phase combustion of pyrolysis products begins. Heat transfer within the particle causes the energy at the surface to move further into the virgin wood. A pyrolysis reaction front develops and this reaction front moves through the particle at a constant velocity, as the energy from the surface of the particle is balanced by the energy used to heat and pyrolyze the virgin wood. The large initial peak in heat release rate is followed by a period of lower heat release rate in which the heat release rate remains fairly constant. The final portion of the heat release rate profile happens as the pyrolysis front reaches the unexposed side of the wooden slab, The heat release profile during this portion of combustion depends on the conditions on the unexposed side of the wooden slab. Cone calorimeter tests have shown that different backing board materials cause changes in the end portion of the heat release rate profile. In some cases a large secondary peak is observed, while in other cases there is little to no secondary peak. The backing board materials tend to reduce or eliminate the secondary peak in the heat release rate. Cone calorimeter data using a backing board is show in Figures 3 and 4.

A comparison of Figures 1-4 shows that the initial peak in heat release rate and the initial peak in pyrolysis gas fluxes depend on the radiant heat flux from the cone calorimeter, and that the backing board does not alter the initial performance of the wooden slab. It took about 15 seconds for sustained ignition for the 50 kW flux cases, and 40 seconds for the 35 kW cases. The peak in pyrolysis gases followed the sustained ignition time by 5 seconds and the highest heat release rate followed the ignition time by 20 seconds for each case. The mass loss peak precedes the heat release rate peak because much of the initial mass loss is due to water vapor leaving the particle, as large fluxes of water vapor inhibit the development and size of a stable flame.

## COMPUTATIONAL MODEL

To gain a better understanding of how boundary conditions on the back side of the wooden slab alter the heat release rate profile, a detailed computational model for biomass pyrolysis was used to examine how backing board materials can alter combustion performance. The computational model is an extension of previous work, in which the wooden slab is discretized onto a one-dimensional grid. Each finite volume initially consists of unreacted wood, liquid water, and water vapor. Conservation of mass, momentum, and energy are applied to each finite volume, and gas flow within the particle is calculated according to Darcy flow. A two-step, competitive pyrolysis scheme allows for variable pyrolysis products. The virgin wood is converted to char, light hydrocarbons and tars by the primary pyrolysis reactions. The secondary pyrolysis reactions account for cracking and repolymerization of the tars. The fraction of each finite volume occupied by solids and gases vary continuously as wood, char, moisture, and pyrolysis gas composition changes. The computational model accounts for shrinkage of the particle due to chemical restructuring. Complete details of the model are given in Hagge and Bryden (2002). Some of the properties used in this model are given in Table 1. The major modifications of the previous model was to link the wood particle to a backing board material. The primary pyrolysis reaction set (1–3)was modeled according to the work of Chan, Kelbon, and Krieger (1985). The tar cracking reaction (4) is from the work of Liden et a1 (1988), while the repolymerization reaction (5) comes from Di Blasi (1993). The total pyrolysis reaction set is as follows.

Primary Pyrolysis Reactions

$$R(1) = 2.0 \cdot 10^{8} \exp\left(\frac{-133000}{8.314 * T}\right) \qquad \text{Wood} \rightarrow \text{Tar}$$

$$R(2) = 1.3 \cdot 10^{8} \exp\left(\frac{-140000}{8.314 * T}\right) \qquad \text{Wood} \rightarrow \text{Gas}$$

$$R(3) = 0.7 \cdot 10^{7} \exp\left(\frac{-121000}{8.314 * T}\right) \qquad \text{Wood} \rightarrow \text{Char}$$

**Secondary Pyrolysis Reactions**

$$R(4) = 4.28 \cdot 10^{6} \exp\left(\frac{-107500}{8.314 * T}\right) \qquad \text{Tar} \rightarrow \text{Gas}$$

$$R(5) = 1.0 \cdot 10^{5} \exp\left(\frac{-107500}{8.314 * T}\right) \qquad \text{Tar} \rightarrow \text{Char}$$

To extend this computational model to the cone calorimeter test, an adequate description of the physical conditions during the cone calorimeter tests is needed. During the cone-calorimeter tests, the surface of the redwood particle is exposed to radiant heat flux from the cone calorimeter, radiant heat transfer from the external gas phase reactions, and to convective heat transfer from the external gases. The radiant energy leaving the cone calorimeter is a known value for each run. The rate of energy released by the combustion gases is measured by the cone calorimeter as the heat release rate. The heat release rate also includes gas phase combustion reactions and char surface reactions (glowing combustion). This glowing combustion occurs only in the latter portion of the cone calorimeter runs after the pyrolysis gas fluxes slow dramatically, and gases can diffuse to the char surface and react with the char layer.

The computational model assumes that the total energy reaching the surface is composed of the radiant energy from the cone calorimeter and the combustion energy from pyrolysis gases and char surface reactions. The pyrolysis gases leaving the particle shield the wooden slab from some of the radiant heat flux. In this model, it is assumed that 5% of the radiation is blocked from reaching the particle when the pyrolysis gas flux is 5g/cm$^2$s. The amount of shielding is based on radiant heat transfer through a participating media, where the fraction of energy reaching the surface is calculated as $\dot{Q}_{surface\bullet} = \dot{Q}_o \exp(- C\dot{m}_{pyr})$. Experimental data shows that the surface receives about 12 kw/m$^2$ from combustion. Based on this, the computational model assumes that 25% of the measured heat release rate is radiated back to the surface, which is consistent with the measured heat flux. The total energy reaching the surface is

$$\dot{Q}_{surface} = \left(\dot{Q}_o + 0.25HRR\right)\exp\left(-C\dot{m}_{pyr}\right)$$

## RESULTS

There is good qualitative relationship between the cone calorimeter data and the computational model. In Figures 5 and 6, the gas fluxes for the computational model are compared with the cone calorimeter. Figures 5 and 6 show the pyrolysis gas fluxes for a cone calorimeter flux of 35kW/m$^2$ and 50kW/m$^2$ when no backing board is used. The computational results predict both a primary and a secondary peak in the rate release of pyrolysis gases. There is generally a good correspondence between the predicted rate of mass loss and the experimental results for each case, although there are some minor differences.

The initial peak in the rate of mass loss for the model corresponds directly to the peak in heat release rate, while the cone calorimeter results show that the peak in mass loss rate precedes the heat release rate peak by about 20 seconds. This difference may be attributed to the fact that in the one-dimensional model, gases can only be driven inward initially, while in the actual wooden slab there is a three-dimensional geometry and gases can escape out of the unheated surfaces. The wood pores near the surface of the wooden slab may also release gases more easily, due to tearing of the wood structure during machining.

The initial peak in mass loss rate is followed by lower, steady rate of pyrolysis gas production. During this portion of combustion, a stable flame has developed. The stable flame produces a fairly constant amount of energy, and the pyrolysis reactions move through the particle at a steady speed. The combustion characteristics of the wooden slab remain constant as the rate of fuel delivery by pyrolysis gases, the rate of oxygen diffusion to the flame, and the rate of combustion of pyrolysis gases find an equilibrium value. During this portion of combustion, the pyrolysis gases are released at a rate of 5 gm/cm$^2$s for a 35 kW/m$^2$ cone calorimeter flux, and a mass loss rate of 7 gm/cm$^2$s is observed with a cone calorimeter flux of 50kW/m$^2$. The numerical results show a slight dip in the rate of production of pyrolysis gases during this steady period. The lowest rate of pyrolysis gas production happens as the pyrolysis gases start to be driven out the back (unheated) side of the wooden slab, rather than out the front of the particle. The difference, although small, is due to the one-dimensional nature of the computational model, and the fact that pyrolysis gases can escape out the sides of the wooden slab.

The secondary peak is predicted by the numerical model. Heat is constantly pulled from the active pyrolysis reaction zone by conduction to the virgin wood further within the particle, As the pyrolysis front nears the back side of the wooden slab, there is less unreacted wood to serve as a heat sink. As a result of the decreasing amount of virgin wood remaining, there is a similar amount of heat transfer into a smaller and smaller area of unreacted wood. This causes the temperature to rise more rapidly when the back side of the wooden slab pyrolyizes, and the higher temperatures cause an increased rate of production of pyrolysis gases. Thus, the secondary peak in mass loss is due to the increased rate of heat transfer into the small, unreacted region on the back side of the wooden slab. The secondary peak is not as pronounced in the computational model as it was with the cone calorimeter data.

A look at the temperature profiles (Figure 7) provides some insight into the differences. For the cases with no backing board, one thermocouple was embedded into the surface of the wooden slab, and one thermocouple was embedded on the back side of the wooden slab. The thermocouple at the surface measured the surface temperature for about the first 100 seconds of the run. After this, the thermocouple would come loose from the surface and could move around. Therefore, the surface thermocouple was only useful for determining the initial response at the surface of the particle. The numerical results are fairly close to the measured results, but predict that the surface of the particle heats up a little more rapidly than the measured temperature. This difference is due to the fact that the thermocouple was imbedded a few millimeters into the surface, rather than measuring the exact surface of the particle.

The predicted temperature at the back side of the wooden slab is very close to the measured temperatures for the first 500 seconds of the run. The computational results differ from this point. The predicted back surface temperature shows a rapid rise in temperature from 400K to 550K. The rapid rise in temperature is caused by the fact that all of the water has been evaporated near the back surface. Once all of the water is gone, there is much less thermal capacity, and the temperatures rise very rapidly. As the specific heat of the wood rises with temperature (Table 1), the rate of increase at the back surface begins to slow. As char formation continues, a steady rate of increase in temperature develops until pyrolysis is complete. The main differences in the temperature profile are that the computational model predicts a rapid increase in temperature from 400K to 550K when all of the water has been driven out of the particle, and that the computational model predicts a more gradual increase in temperature from this point. This difference may be due to the importance of recondensation of water vapor. As hot pyrolysis gases are driven out of the back surface of the particle, they travel through a cooler surface. Water vapor that was either evaporated or produced during pyrolysis reactions can condense on the cooler surface. Recondensation has been shown to be more important for low moisture contents, as water is more tightly bound within wood pores at low moisture contents, The back surface temperature matches the cone calorimeter data during the secondary peak. The computational model predicts a sharper initial increase in temperature once the particle is dry, followed by a more gradual increase in temperature. This more gradual increase in temperature in the model causes pyrolysis to happen over a longer period of time at lower temperatures. As a result, the secondary peak is not as pronounced in the numerical model. After pyrolysis is complete, the numerical model predicts a rapid rise in temperature, while the experimental data shows a much more gradual increase in temperature. The secondary peak ends more abruptly in the numerical model because of the final rapid rise in temperature, and because the computational model does not include gas fluxes due to the char surface reactions. Char reactions begin only after pyrolysis is complete, and the small heat release rate and mass loss rate after the secondary peak is due to these char surface reactions.

The pyrolysis gas fluxes for the backing board cases are shown in Figures 8 and 9. With the presence of the ASTM E84 backing board, the secondary peak is completely eliminated for both cone calorimeter heat fluxes. The initial response of the wooden slab is identical to the case where there is no backing board.

The presence of the backing board causes an additional heat sink at the back of the particle. With no backing board, a piece of foil absorbs very little energy and radiates back to the particle. When a backing board is present, it has a much higher thermal capacity, and more energy is transferred form the back side of the wooden slab to the backing board. This causes some backing board materials to dramatically reduce the rate of increase in temperature near the back surface of the particle, and can eliminate the secondary peak in pyrolysis gases shown for the no backing board cases.

## CONCLUSIONS

The computational model has been used to demonstrate how backing board materials can alter combustion performance. The model predicts a secondary peak when no backing board is present, but the sue of the secondary peak is somewhat smaller than what is measured by the cone calorimeter. This difference is likely due to the affect of recondensation of water vapor on the back side of the wooden slab, as hot water vapor is driven across cooler surfaces. Additional water on the back surface will cause a sharper increase in the rate of temperature increase once the particle is completely dried. This sharper increase in temperatures will cause additional pyrolysis gases to be produced, and will increase the size of the secondary peak. The numerical model has been able to predict qualitatively what happens when a backing board material is present during combustion.

Future work consists of applying several different backing board materials in the computational model to the redwood slab. This can be done without performing additional cone calorimeter runs for each backing material. Because the initial response of the wooden slab is not influenced by the backing board, the heat release rate from previous cone calorimeter tests for a given heat flux can be used for the primary peak for any backing board material. The close correlation between heat flux and mass loss rate indicates that the heat release rate ($kW/m^2$) will be between 10 to 12 times that of the mass flux ($g/cm^2s$). Future work will rely on using a pyrolysis model in which the heat release rate after the primary peak is a function of pyrolysis gas fluxes. This should allow the investigation of new backing board materials without requiring cone calorimeter heat release measurements for every possible backing material.

**Table 1. Values and correlations used**

| Property | Correlation/Value | Ref |
|---|---|---|
| Void Fraction | $\varepsilon = 1 - (\rho_w + \rho_C)/1500 - \rho_m/1000$ | Siau, 1984 |
| Permeability | $\phi = \eta\phi_W + (1-\eta)\phi_C$ where $\eta = m_W / m_{W,O}$ | |
| | $\phi_w = 1 \times 10^{-2}$ darcys | Bryden, 1998 |
| | $\phi_c = 1$ darcys | Bryden, 1998 |
| Thermal Conductivity | $\lambda_{eff} = \lambda_{cond} + \lambda_{rad}$ | |
| | $\lambda_{rad} = \varepsilon/(1-\varepsilon)\sigma\varphi_p d_p 4T^3$ | Panton and Rittman, 1971 |
| | $\varphi_p = 0.9$ | |
| | $\lambda_{cond} = \lambda_M + \eta\lambda_W + (1-\eta)\lambda_C$ | |
| | $\lambda_W = 0.200 \cdot X + 0.0238 \left(\mathrm{W\,m^{-1}\,K^{-1}}\right)$ | Forest Product Lab, I987 |
| | $\lambda_M = X(0.0040 \cdot M)\left(\mathrm{W\,m^{-1}\,K^{-1}}\right)$ | Forest Product Lab, 1987 |
| | $\lambda_C = 0.105\ \mathrm{W\,m^{-1}\,K^{-1}}$ | Lee et al, 1974 |

**Continued Table 1.**

| Property | Correlation/Value | Ref |
|---|---|---|
| Specific Heat | $c_W = 0.003867(T - 273.2) + 0.1031 \left(\frac{\text{kJ}}{\text{kgK}}\right)$ | TenWolde et al, 1988 |
| | $c_C = 1.39 + 0.00036T \left(\text{kJ kg}^{-1}\text{ K}^{-1}\right)$ | Stull,1971 |
| | $c_{pyr} = 2.4\ \text{kJ kg}^{-1}\text{ K}^{-1}$ | Bryden, 1998 |
| | $c_M = 4.18\ \text{kJ kg}^{-1}\text{ K}^{-1}$ | Borman and Ragland 1998 |
| Molecular Weight | $W_V = 18 \times 10^{-2}\ \text{kg mol}^{-1}$ | Borman and Ragland 1998 |
| | $W_L = 26 \times 10^{-2}\ \text{kg mol}^{-1}$ | Bryden, 1998 |
| | $W_V = 110 \times 10^{-2}\ \text{kg mol}^{-1}$ | Bryden, 1998 |
| Dynamic Viscosity | $\mu = 4.847 \cdot 10^{-7} T^{0.64487} \left(\text{kg m}^{-1}\text{ s}^{-1}\right)$ | Bryden, 1998 |
| Heat Transfer Coefficient | $h_{rad} = \varphi\sigma \frac{1}{2}(T_s + T_\infty)(T_s^2 + T_\infty^2)$ where $T_s = T_\infty$ | Bryden, 1998 |

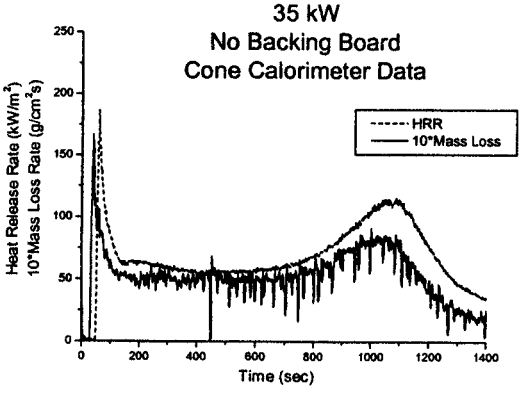

Figure 1

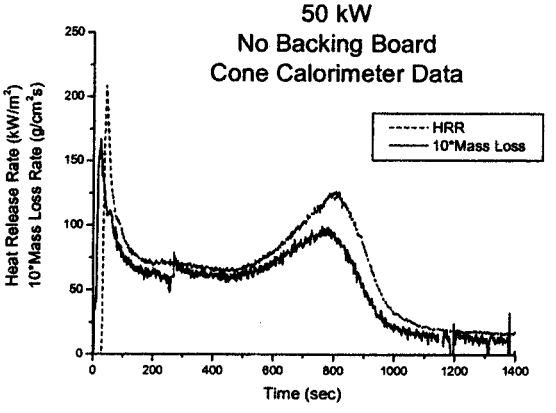

Figure 2

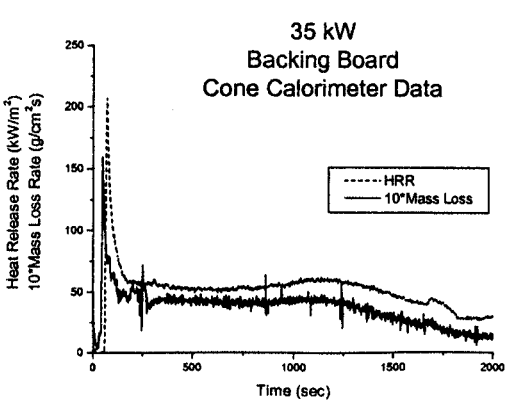

Figure 3

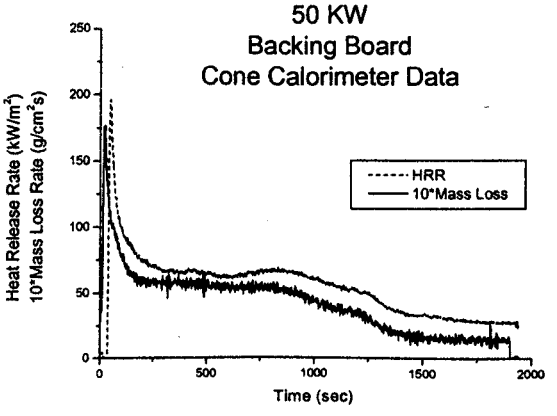

Figure 4

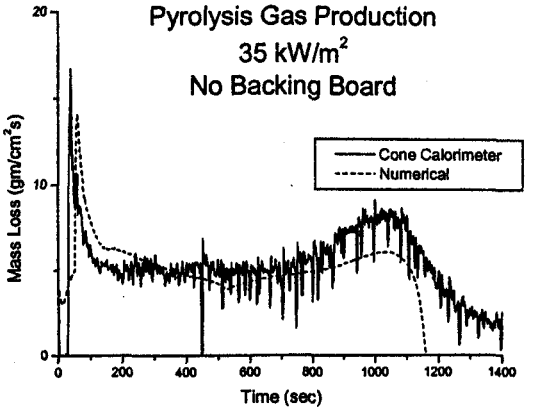


Figure 5

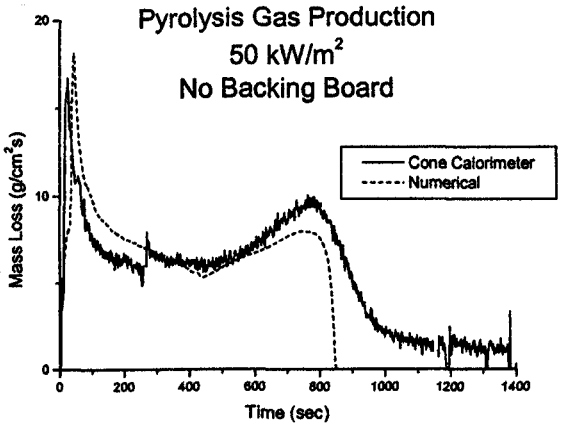


Figure 6

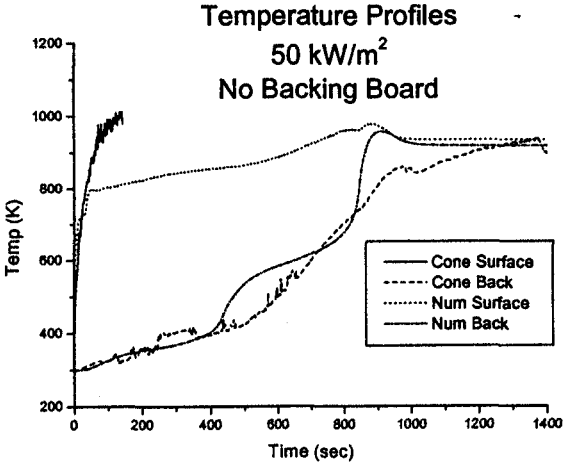


Figure 7

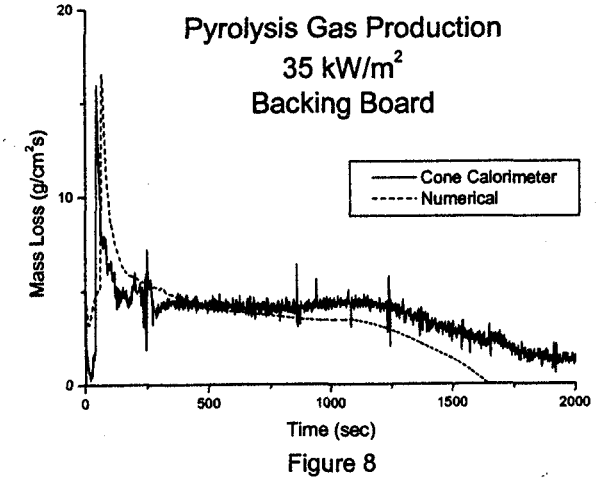


Figure 8

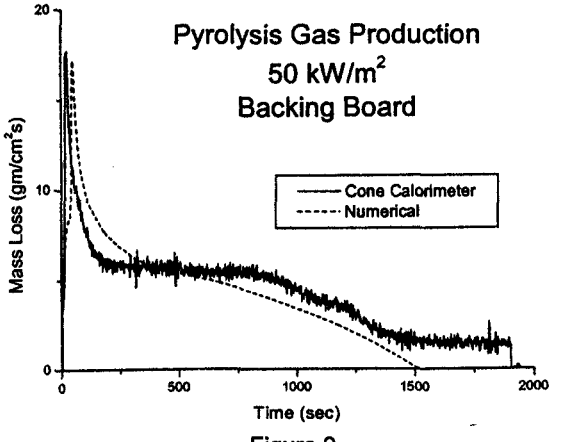


Figure 9

## REFERENCES

Borman, G. L., Ragland, K. W. 1998. *Combustion Engineering.* McGraw-Hill, NewYork.

Bryden, K. M. 1998. Computational Modeling of Wood Combustion. Ph. D. Thesis, University of Wisconsin-Madison.

Chan, W. R., Kelbon, M., Krieger, B. B. 1985. Modeling and experimental verification of physical and chemical processes during pyrolysis of a large biomass particle. *Fuel,* 64, p 1505–1513.

Di Blasi, C. 1993. Analysis of convection and secondary reaction effects within porous solid fuels undergoing pyrolysis. *Combustion Science and Technology*, 90, p 3 15–340.

Dietenberger, M. 1999. Effect of Backing Board on the Heat Release Rate of Wood. Proceedings of the *International Conference on Fire Safety*, July 1999, p 62–73.

Forest Products Laboratory 1987. *Wood Handbook: Wood as an Engineering Material Agricultural Handbook* 72. U.S. Department of Agriculture, Washington, DC.

Hagge, M., Bryden, K. M. 2002. Modeling the impact of shrinkage on the pyrolysis of dry biomass. *Chemical Engineering Science*, v57, n14, July 2002, p 281 1–2823.

Lee, C. K., Chaiken, R. F., Singer, J. M. 1976. Charring pyrolysis of wood in fires by laser simulation. *Sixteenth Symposium (International) on Combustion.* p 1459–1470. The Combustion Institute, Pittsburgh.

Liden, A. G., Berruti F., Scott D. S. 1988. A kinetic model for the production of liquids from the flash pyrolysis of biomass. *Chemical Engineering Communications*, 65, p 207–221.

Panton, R. L., Rittman, J. G. 1971. Pyrolysis of a slab of porous material. *Thirteenth Symposium (International) on Combustion.* p 881–891. The Combustion Institute, Pittsburgh.

Siau, F. F. 1984. *Transport Processes in Wood.* Springer Verlag, New York.

Stull, D. R. 1971. *JANAF Thermochemical Tables, NSRDS-NBS 37.* US Government Printing Office.

TenWolde, A., McNatt, J. D., Krahn, L. 1988. Thermal Properties of Wood and Wood Panel Products for Use in Buildings, DOE/USDA-21697/1. Oak Ridge National Laboratory, Oak Ridge.

**Address:**

Mathew Hagge Keneth M. Bryden
1620 Howe Hall
2274 Iowa State University
Ames, IA 50011
fforty@iastate.edu

Mark A. Dietenberger, Ph.D.
USDA Forest Service – Forest Products Laboratory
Madison, WI 53726, USA.

# WOOD & FIRE SAFETY

## DREVO A PROTIPOŽIARNA BEZPEČNOSŤ

5th International Scientific Conference
April 18-22, 2004
Štrbské Pleso, The Patria Hotel
Slovak Republic

# PROCEEDINGS




5. 03. 04